Supplementary Materials

Liquid metal-based dynamic conformal electrodes

Xiaotong Liu[1,#], Chunxue Wan[2,#], Jiaping Liu[3,#], Hui Xu[1], Yubing Liu[2], Yi Liu[4], Yanqing Liu[1], Jing Liu[2], Hongzhang Wang[5,6], Haojun Fan[1,*], Rui Guo[2,3,*]

[1]School of Disaster and Emergency Medicine, Tianjin University, Tianjin 300072, China.
[2]State Key Laboratory of Cryogenic Science and Technology, Technical Institute of Physics and Chemistry, Chinese Academy of Sciences, Beijing 100190, China.
[3]School of Precision Instrument and Opto-Electronics Engineering, Tianjin University, Tianjin 300072, China.
[4]Key Laboratory for Biomechanics and Mechanobiology of the Ministry of Education, School of Engineering Medicine, Beihang University, Beijing 100191, China.
[5]Institute of Materials Research & Center of Double Helix, Shenzhen International Graduate School, Tsinghua University, Shenzhen 518055, Guangdong, China.
[6]The Key Laboratory of Bionic Engineering (Ministry of Education), Jilin University, Changchun 130022, Jilin, China.
[#]Authors contributed equally.

[*]**Correspondence to:** Haojun Fan, School of Disaster and Emergency Medicine, Tianjin University, No. 92 Weijin Road, Tianjin 300072, China. E-mail: fanhj@tju.edu.cn; Rui Guo, State Key Laboratory of Cryogenic Science and Technology, Technical Institute of Physics and Chemistry, Chinese Academy of Sciences, No. 29 Zhongguancun East Road, Haidian District, Beijing 100190, China. E-mail: guorui@mail.ipc.ac.cn

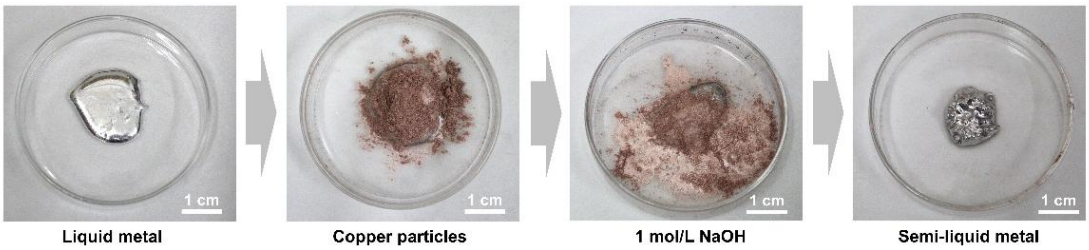

Supplementary Figure 1. Pictures of the preparation method of SLM.

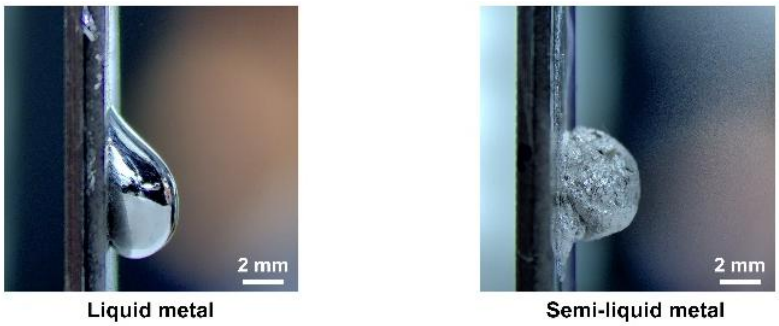

Supplementary Figure 2. Pictures showing the fluidity difference between liquid metal and SLM.

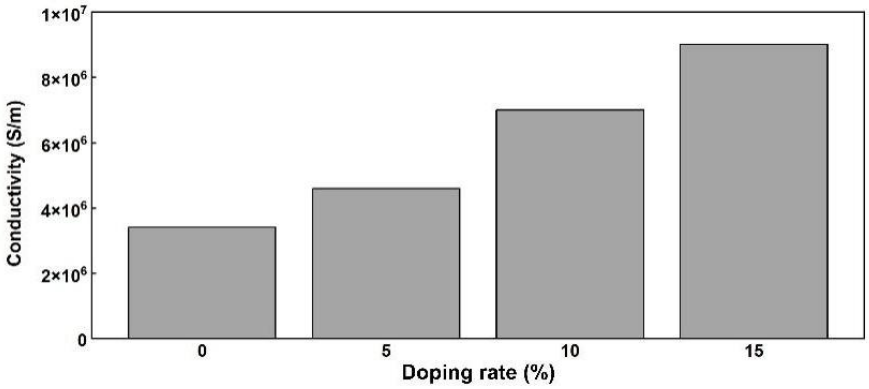

Supplementary Figure 3. The electrical conductivity of SLM with different doping ratios.

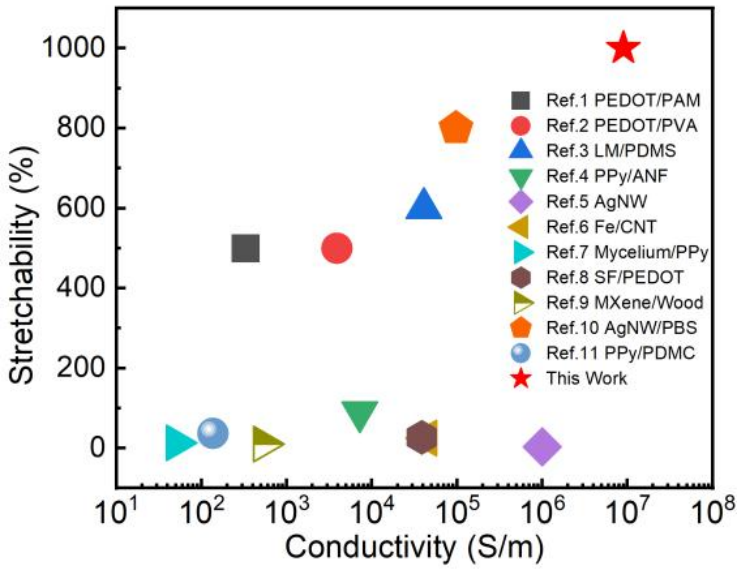

Supplementary Figure 4. Comparison of conductivity to that of previously reported stretchable conductors at maximum stretchability.

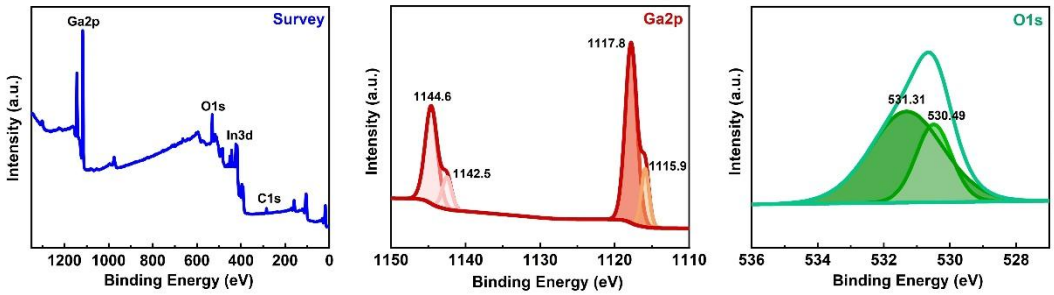

Supplementary Figure 5. XPS curves of the oxide film on the surface of SLM.

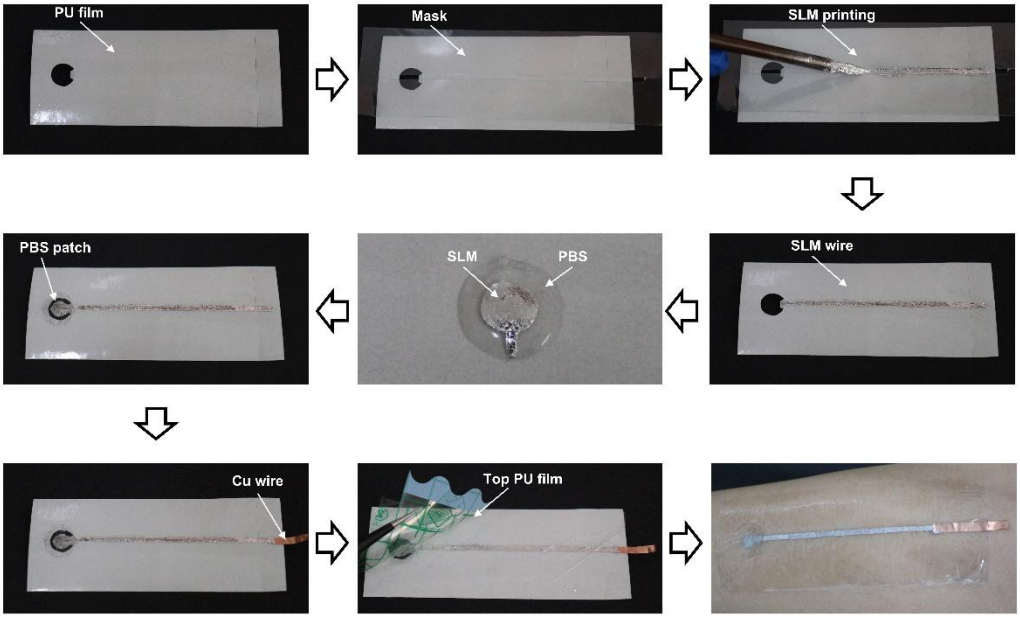

Supplementary Figure 6. Pictures showing the manufacturing method of the electrode system.

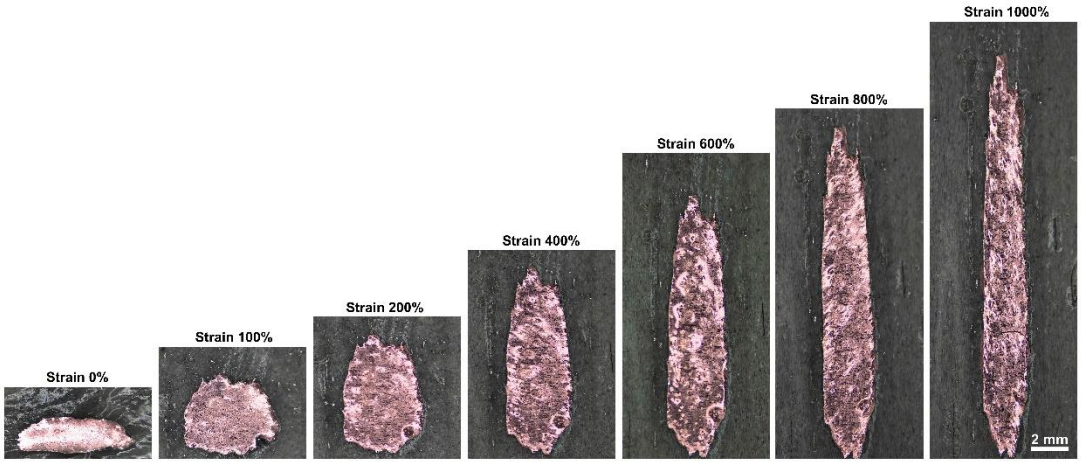

Supplementary Figure 7. Pictures of SLM following the stretching of the PBS substrate.

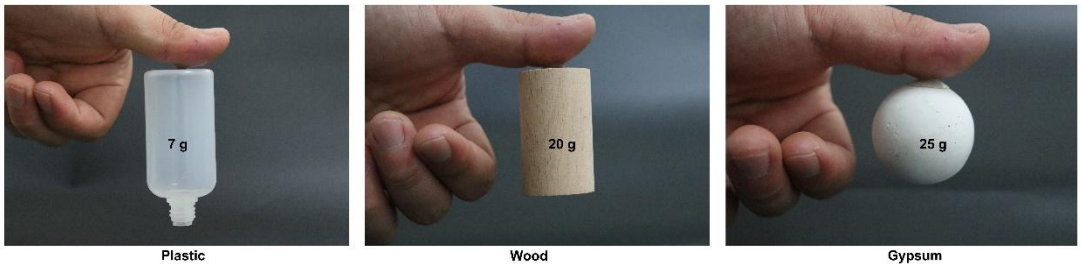

Supplementary Figure 8. Pictures showing the high adhesion of PBS to objects made of different materials.

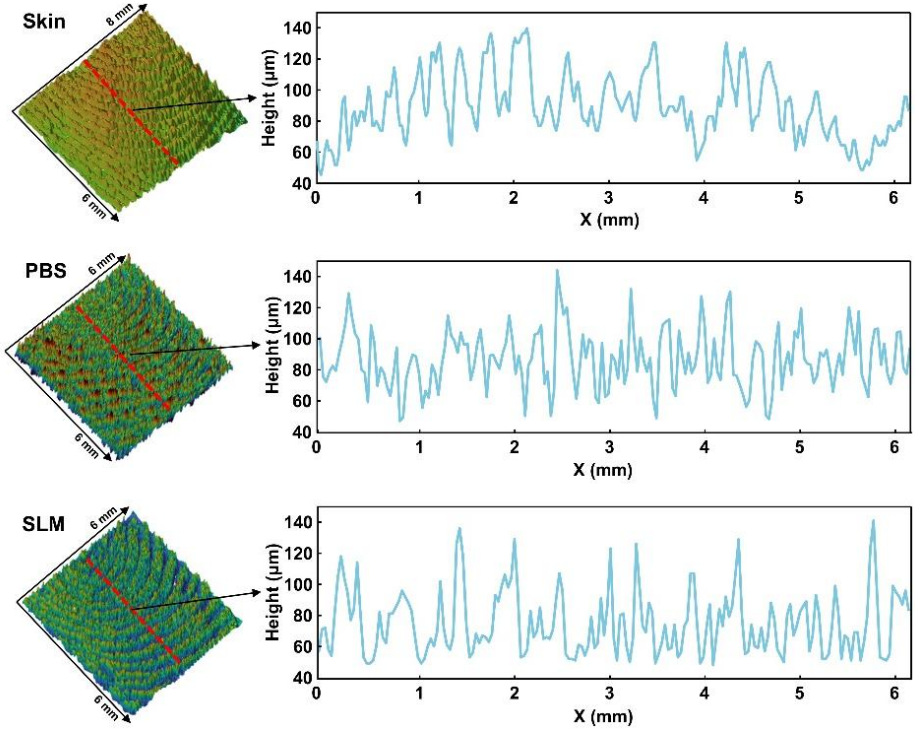

Supplementary Figure 9. Topography contour curves of skin, PBS, and SLM.

Supplementary Figure 10. Pictures showing that the SLM-PBS electrode is easy to peel off from the skin, and will not leak out under pressure or tensile strain.

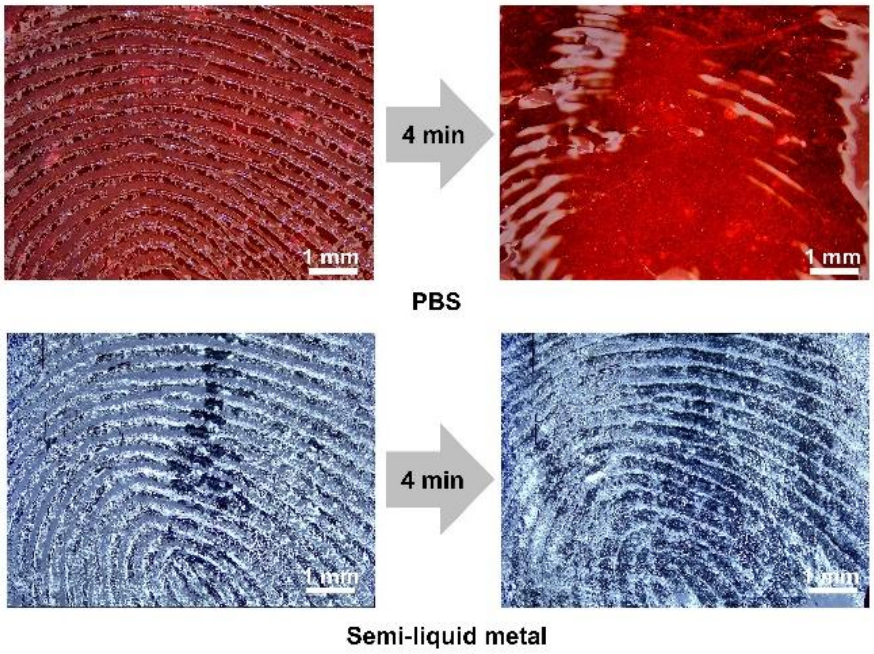

Supplementary Figure 11. Pictures showing the disappearance of skin textures on PBS and SLM.

Supplementary Figure 12. The self-built multifunctional mechanical-electrical coupling testing platform.

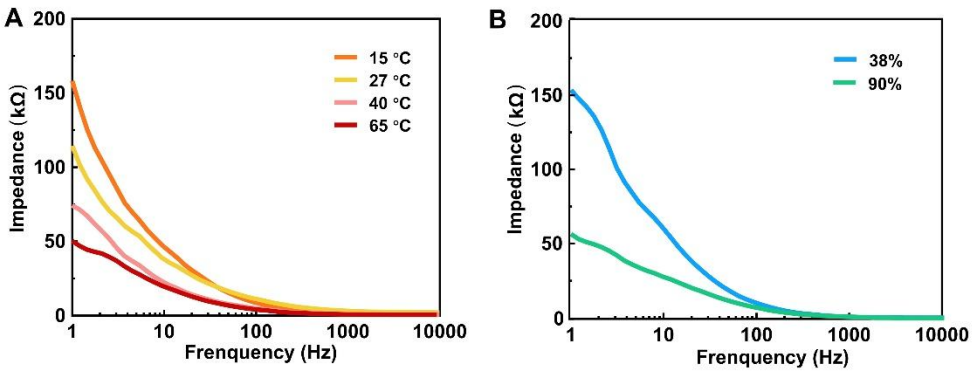

Supplementary Figure 13. The impedance-frequency characteristics of the SLM-PBS electrode at different temperatures and humidity.

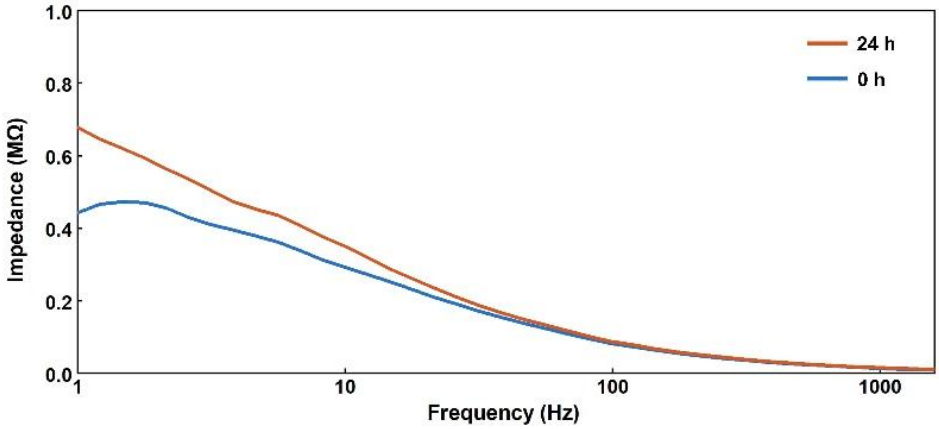

Supplementary Figure 14. The impedance-frequency characteristics of the SLM-PBS electrode before and after 24 h.

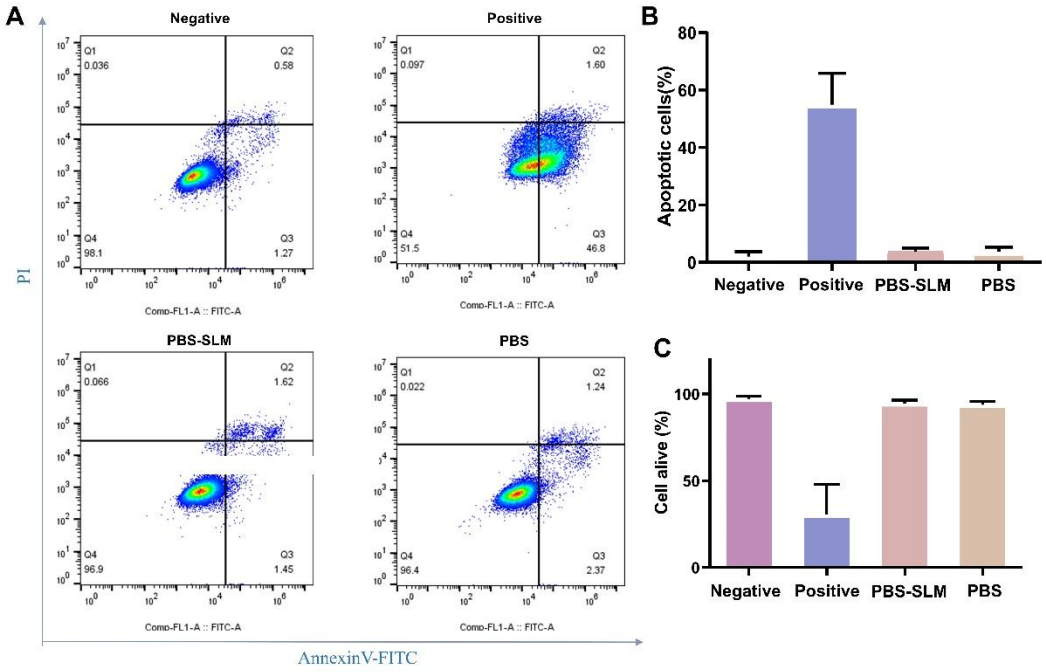

Supplementary Figure 15. Flow cytometry testing of PBS and SLM-PBS materials for apoptosis experiments. (A) Flow cytometry results of cells from PBS, SLM-PBS, blank group, and 4%PFA positive group;(N>3) Q1 represents cell necrosis (AnnexinV-/PI+); Q2 represents late apoptotic cells (AnnexinV+/PI+); Q3 represents early apoptotic cells (AnnexinV+/PI-); Q4 represents normal cells (AnnexinV-/PI-). (B) Statistics of apoptosis rates in different groups in panel A. (C) Statistics of cell viability in different groups in panel A.

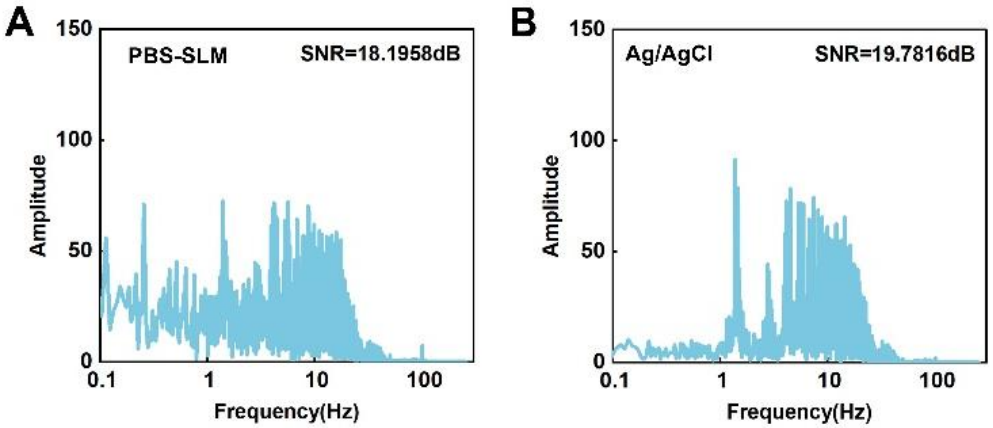

Supplementary Figure 16. The SNRs of the signals collected by the SLM-PBS electrode and the Ag/AgCl electrode.

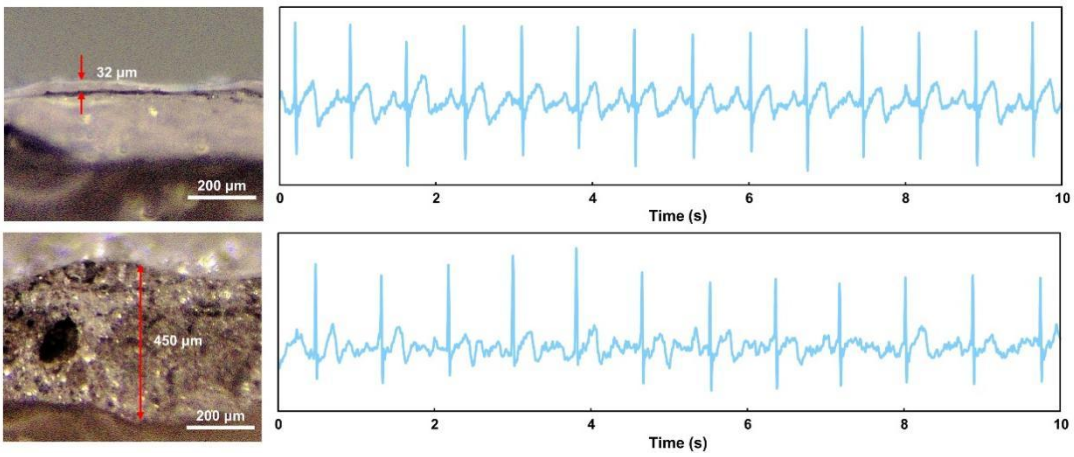

Supplementary Figure 17. Cross-sectional images of thin and thick electrodes and their detected ECG signals.

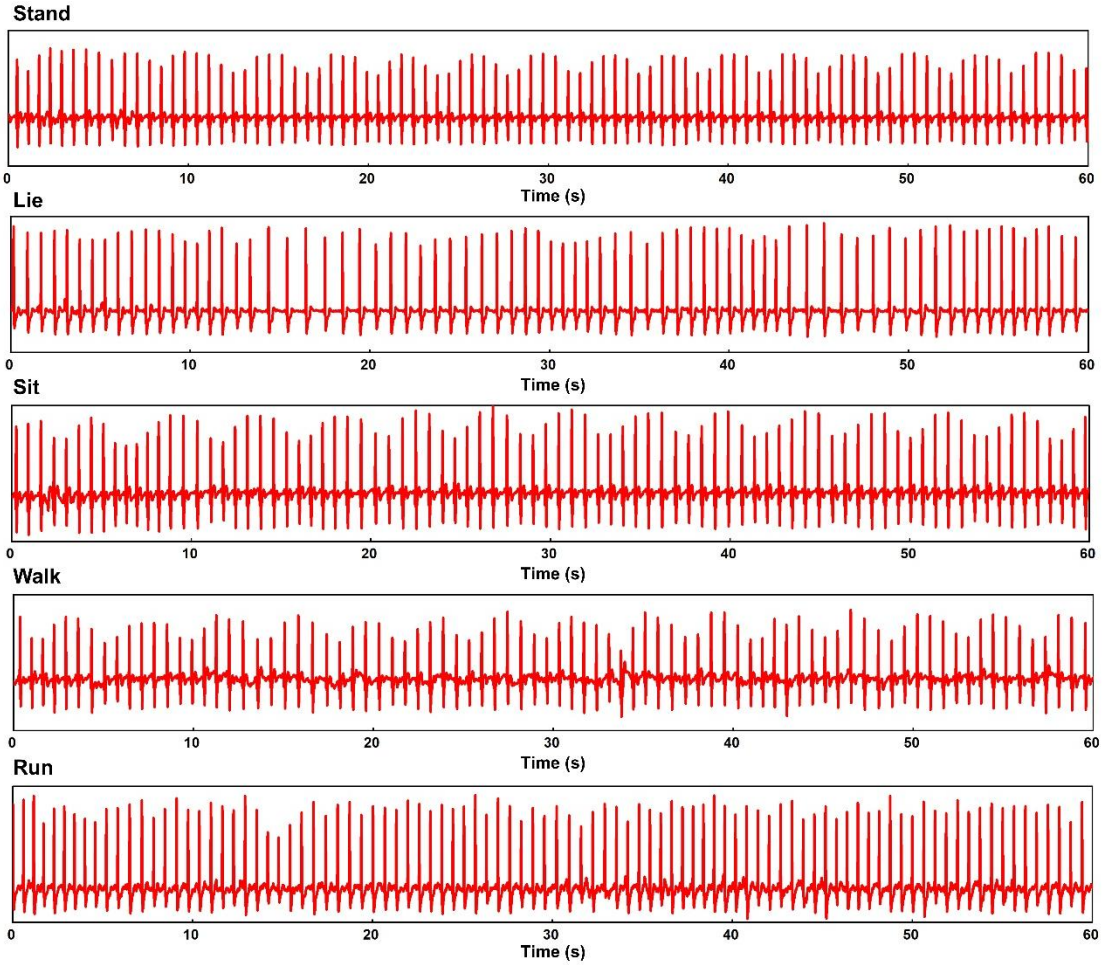

Supplementary Figure 18. ECG signals within 1 min under different postures.

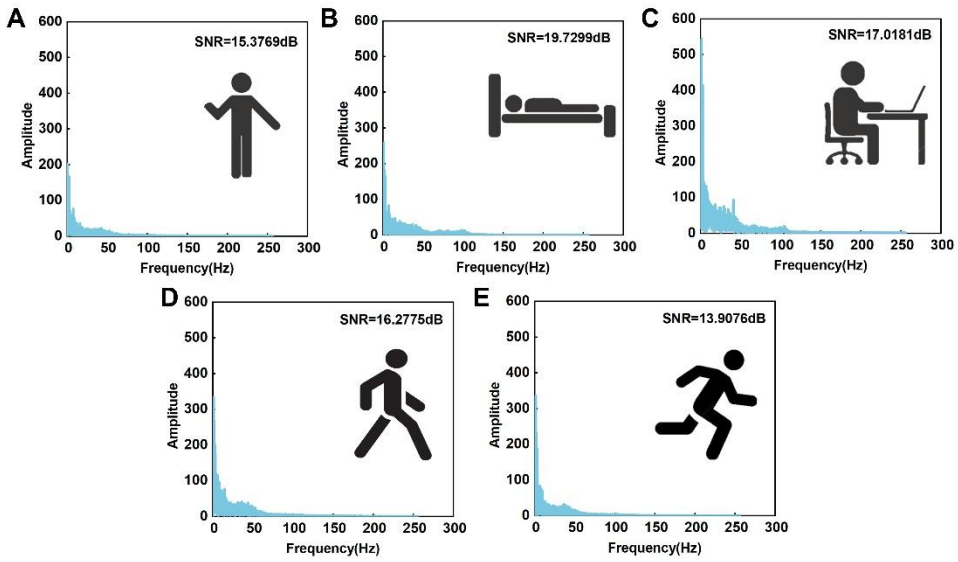

Supplementary Figure 19. The SNRs of the ECG signals collected under different postures.

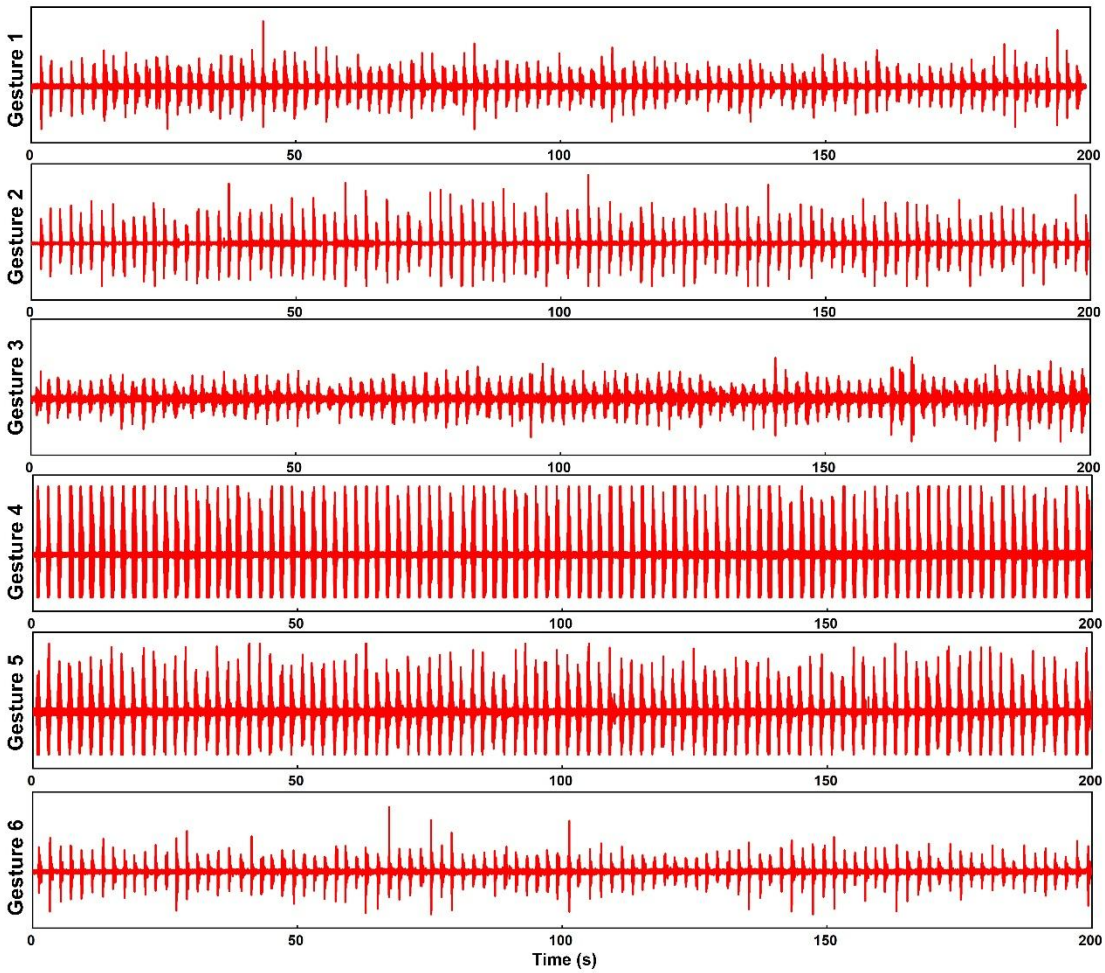

Supplementary Figure 20. The EMG signals of six kinds of gestures collected by Electrode Pair 1.

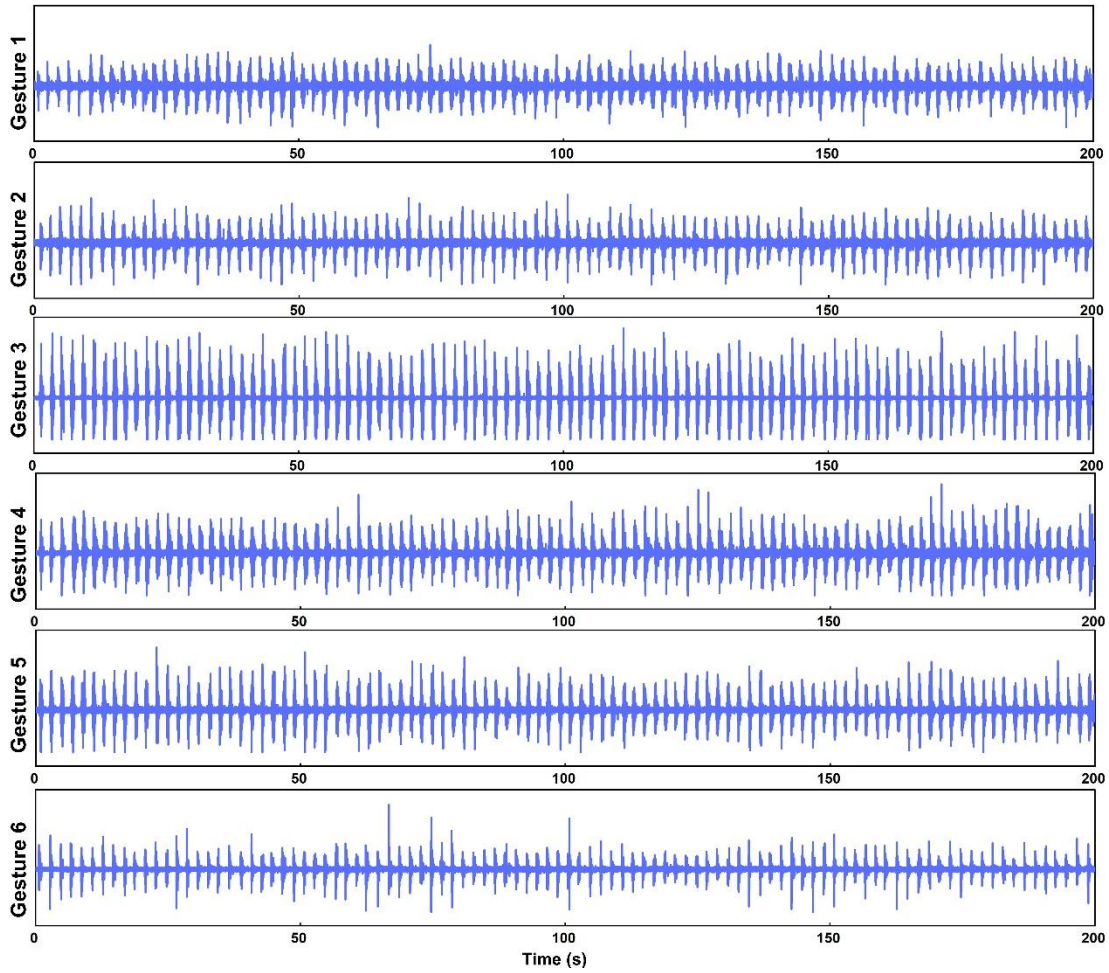

Supplementary Figure 21. The EMG signals of six kinds of gestures collected by Electrode Pair 2.

Supplementary Video 1. The SLM-PBS electrode applied on the skin.

Supplementary Video 2. The SLM wire applied on the skin.

Supplementary Video 3. SLM deforms with the stretching of the PBS substrate.

REFERENCES

[1] Zhao Y, Chen S, Hu J, et al. Microgel-Enhanced Double Network Hydrogel Electrode with High Conductivity and Stability for Intrinsically Stretchable and Flexible All-Gel-State Supercapacitor[J]. ACS Applied Materials & Interfaces, 2018, 10(23): 19323-19330.

[2] Kolathodi M S, Akbarinejad A, Tollemache C, et al. Highly stretchable and flexible supercapacitors based on electrospun PEDOT:SSEBS electrodes[J]. Journal of Materials Chemistry A, 2022, 10(39): 21124-21134.

[3] Zhang J-R, Li A, Li X-L, et al. High-Resolution Stretchable Soft Liquid Metal Circuits Based on Cu–Ga Alloying and Femtosecond Laser Ablation[J]. ACS Applied Materials & Interfaces, 2025, 17(12): 18940-18953.

[4] He H, Chen Y, Pu A, et al. Strong and high-conductivity hydrogels with all-polymer nanofibrous networks for applications as high-capacitance flexible electrodes[J]. npj Flexible Electronics, 2024, 8(1): 56.

[5] Tang C, Zhang K, Yu S, et al. All-Metal Flexible Fiber by Continuously Assembling Nanowires for High Electrical Conductivity[J]. Small, 2024, 20(46): 2405000.

[6] Wang Y, Liang W, Hao D, et al. Flexible, Stable, and Efficient Counter Electrode for Quantum-Dot-Sensitized Solar Cells Based on Carbon Nanotube Films[J]. ACS Applied Materials & Interfaces, 2024, 16(27): 35474-35483.

[7] Zhang R, Cheng S, Pan Z, et al. Biovegan Leather Sensor: A Mycelium Functionalized Material for Electrophysiological Signal Monitoring[J]. ACS Applied Materials & Interfaces, 2025, 17(23): 34538-34547.

[8] Hu Z, Liang Y, Fan S, et al. Flexible Neural Interface From Non-Transient Silk Fibroin With Outstanding Conformality, Biocompatibility, and Bioelectric Conductivity[J]. Advanced Materials, 2024, 36(46): 2410007.

[9] Zhu S, Chen M, Wang S, et al. 3D oxidation-resistant MXene electrode supported by softened wood toward high-performance flexible supercapacitors[J]. Chemical Engineering Journal, 2024, 496: 153739.

[10] Wan C, Feng Z, Gao Y, et al. Self-Healing and Shear-Stiffening Electrodes for Wearable Biopotential Sensing and Gesture Recognition[J]. ACS Sensors, 2024, 9(10): 5253-5263.

[11] Guan M, Han Z, Liu N, et al. Electrical percolation network based on nano-cellulose template for flexible hydrogel bioelectrode[J]. Carbohydrate Polymers, 2025, 362: 123693.